# Additional file 1

## Supplementary figures and tables

A biphasic astrocytic PTGDS trajectory marks a metabolic vulnerability stage in prodromal Alzheimer's disease

Figures S1–S8 and Tables S1–S10. Table S10 is additionally provided as a machine-readable spreadsheet in Additional file 2.

**Fig. S1**

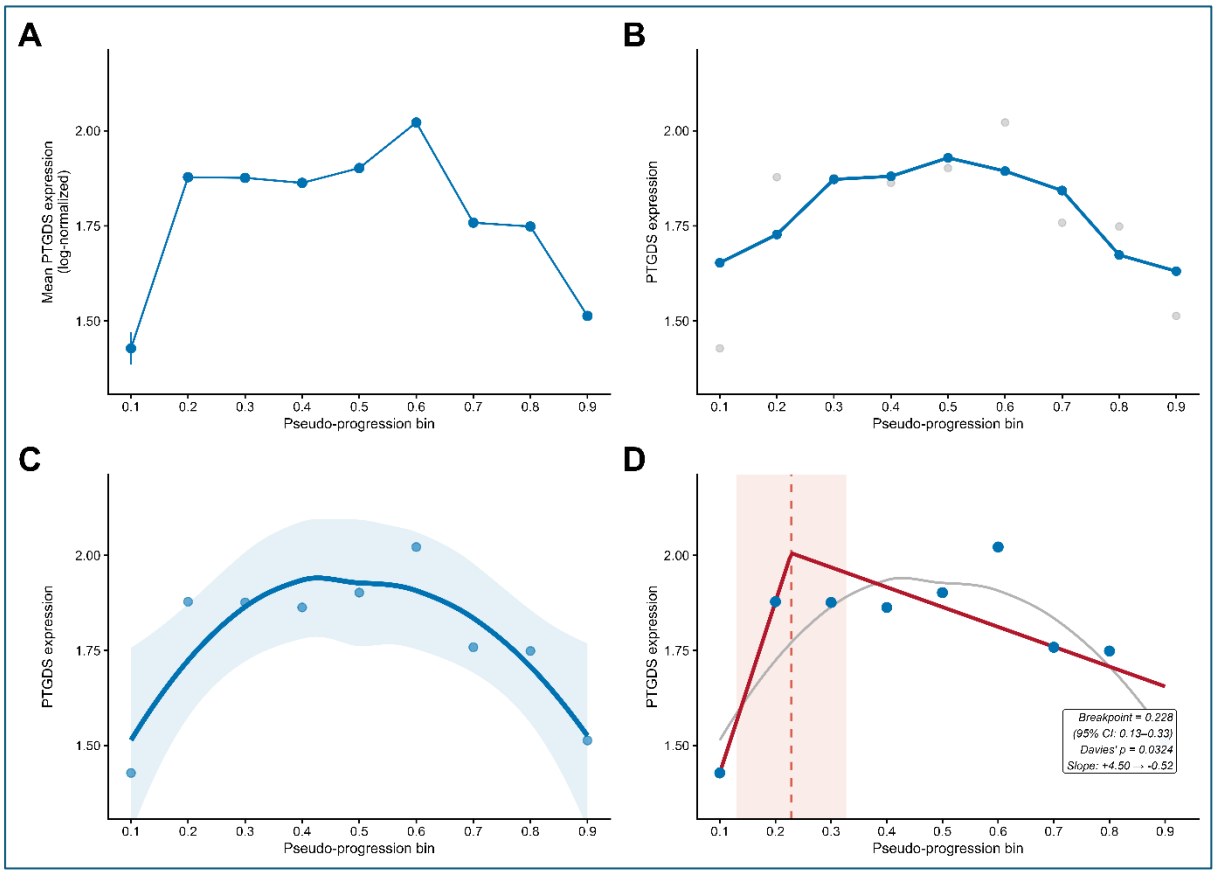


***Statistical validation of the biphasic PTGDS trajectory and inflection point.*** ***A.*** *Unsmoothed bin-level mean PTGDS expression (± SEM) across nine pseudo-progression bins (Bins 0.1–0.9) in SEA-AD astrocytes. The raw trajectory shows an initial rise from Bin 0.1 to a peak at Bin 0.6 (raw mean = 2.02), followed by progressive decline.* ***B.*** *Three-bin centered moving average (blue) used for lagged cross-correlation analyses (Table 3). Gray points indicate unsmoothed values.* ***C.*** *LOESS regression (span = 1.0) with 95% confidence interval confirming the biphasic trajectory: compensatory upregulation through mid-progression followed by exhaustion-phase decline.* ***D.*** *Segmented regression identifying a statistically significant slope change (breakpoint) at Bin 0.23 (95% CI: 0.13–0.33; Davies' test p = 0.032), with a steep ascending slope (+4.50) preceding the breakpoint and a gradual declining slope (−0.52) thereafter. The gray curve shows the LOESS fit for reference. *Data derived from astrocytes (n = 428–14,108 cells per bin) across 84 SEA-AD donors.*

**Fig. S2**

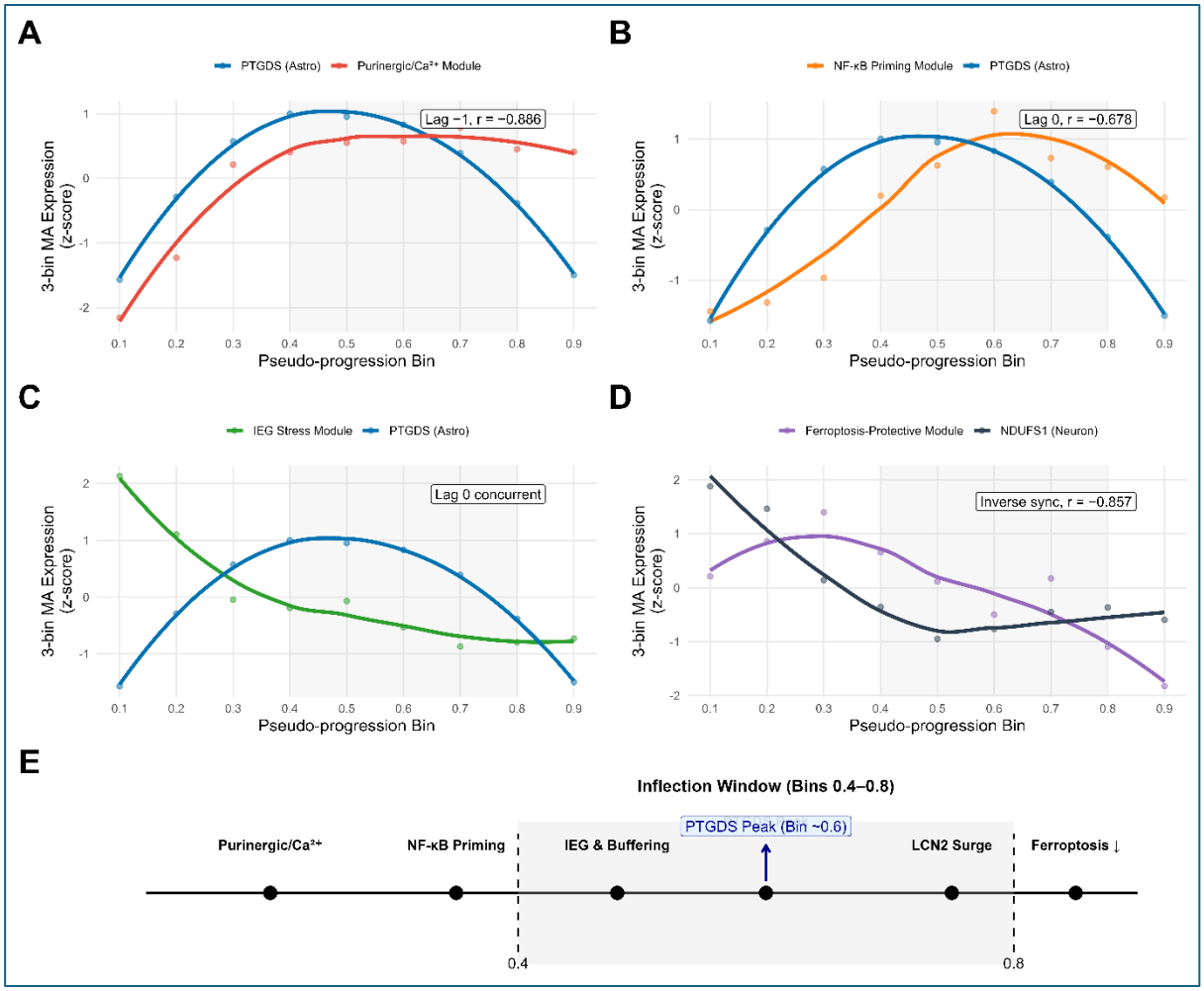


***Module-level mechanistic dissection of the astrocyte–neuron cascade in SEA-AD pseudo-progression.*** *Module-level trajectories of key astrocyte programs relative to PTGDS across pseudo-progression bins (3-bin moving average of log-normalized expression). The inflection window (Bins 0.4–0.8) is highlighted in gray. Lagged cross-correlation values are indicated in boxed annotations.* ***A.*** *Purinergic/$Ca^{2+}$ module leads PTGDS by one bin (Lag −1, r = −0.886), indicating sensing–compensation coupling.* ***B.*** *NF-κB priming module shows concurrent to modestly leading dynamics with PTGDS (Lag 0, r = −0.678 within inflection window; Lag −1, r = −0.706 across full trajectory), representing inflammatory priming associated with PTGDS modulation.* ***C.*** *Immediate early gene (IEG) stress module shows concurrent trajectory with PTGDS (Lag 0), reflecting tight compensatory coupling.* ***D.*** *Ferroptosis-protective module declines in parallel with loss of neuronal NDUFS1, consistent with coordinated metabolic–trophic stress across the inflection window.* ***E.*** *Temporal sequence of module activation along pseudo-progression, highlighting the inflection window (Bins 0.4–0.8) with dashed lines. PTGDS peak occurs at Bin ~0.6, demarcating the transition from compensatory to post-inflection destabilization phase. Expression values are z-score normalized within each trajectory to enable direct visual comparison of relative temporal dynamics across modules with different absolute expression levels. Lagged cross-correlation values refer to the inflection window analysis (Bins 0.4–0.8; Table 3).*

**Fig. S3**

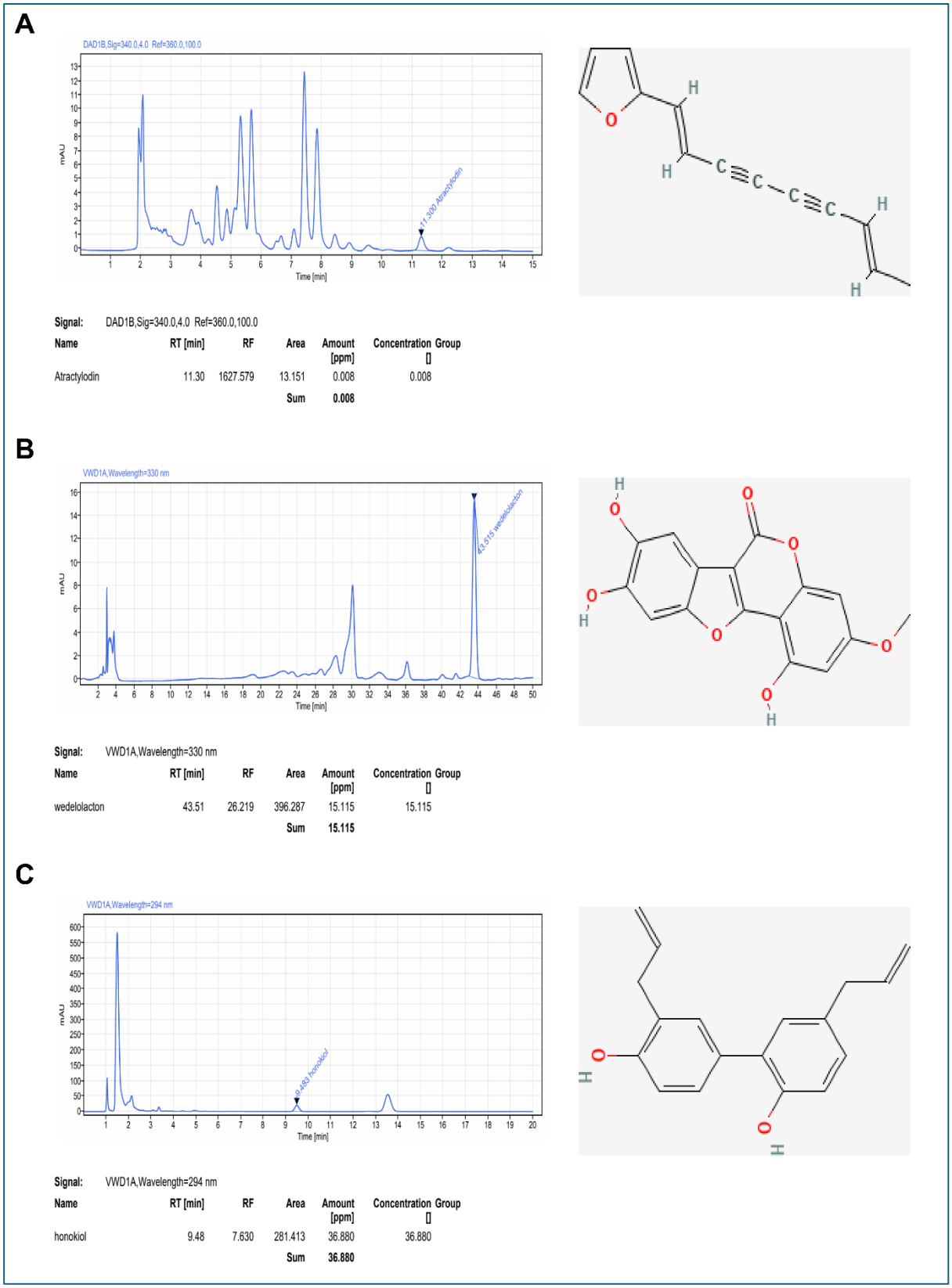


***Chemical standardization of BXP-101. HPLC-DAD chromatograms and chemical structures of the three major marker compounds in BXP-101: A.*** *Atractylodin,* ***B.*** *Wedelolactone, and* ***C.*** *Honokiol. The*

*tables below each chromatogram summarize the retention time (RT), peak area, and standardized concentration groups, ensuring batch-to-batch chemical consistency of the multi-component formulation.*

**Fig. S4**

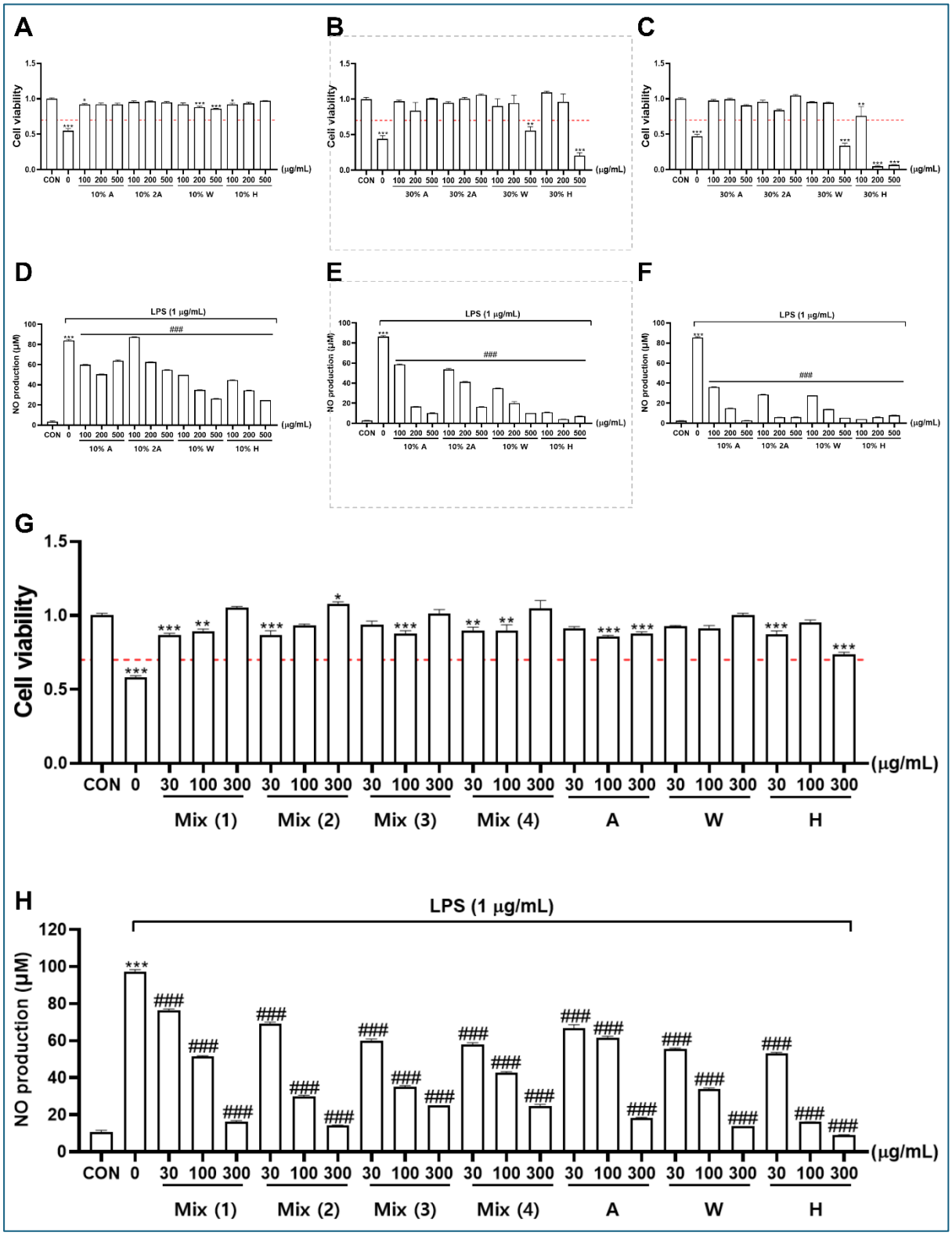

***In vitro validation of BXP-101: Non-cytotoxic anti-inflammatory synergy in BV-2 microglia. A–C.*** *MTT cell viability assays for individual constituents (Atractylodin, Wedelolactone, Honokiol) in BV-2 cells (100–500 μg/mL). The red dashed line denotes the 70% viability threshold for non-toxicity.* ***D–F.*** *Dose-dependent inhibition of LPS-induced (1 μg/mL) nitric oxide (NO) production by individual constituents.* ***G.*** *Comparative viability of BV-2 cells treated with BXP-101 Mix (1–4) vs. single components, showing preserved viability up to 300 μg/mL for the optimized Mix (4).* ***H.*** *Synergistic anti-inflammatory effect of BXP-101 Mix (4) at 300 μg/mL, significantly outperforming individual constituents in suppressing NO production. Data represent mean ± SEM (n = 3 independent experiments). Statistical significance was determined by one-way ANOVA with Tukey's post-hoc test. *p < 0.05, **p < 0.01, ***p < 0.001 vs. Control (CON); ###p < 0.001 vs. LPS-only group.*

**Fig. S5**

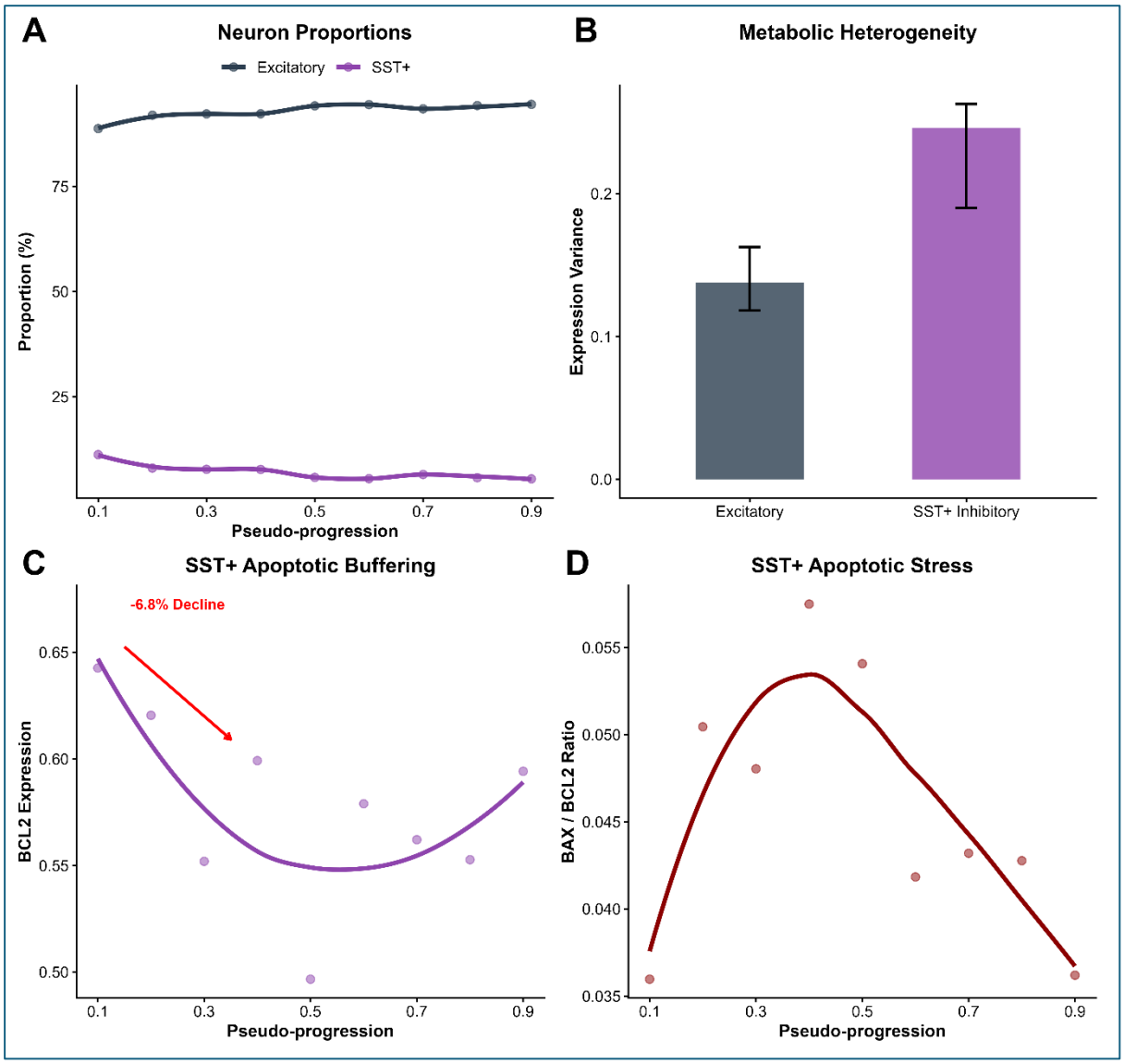


***Differential vulnerability and apoptotic buffering capacity across neuronal subtypes. A.*** *Proportional changes of excitatory neurons and SST$^+$ inhibitory interneurons across pseudo-progression bins. SST$^+$ neurons exhibit a progressive decline (from 11.24% to 5.49% as a fraction of excitatory + SST neurons*

*(donor-level Spearman ρ = −0.32, p = 0.003)), while excitatory neuron proportion increases correspondingly.* ***B.*** *Comparison of NDUFS1 expression variance, reflecting increased metabolic heterogeneity in SST⁺ neurons under post-inflection stress.* ***C.*** *Trajectory of anti-apoptotic marker BCL2 in SST⁺ neurons, showing a 6.8% decline during the early window (Bins 0.1–0.4).* ***D.*** *Early elevation of the BAX/BCL2 ratio within the SST⁺ population, indicating transient apoptotic stress and diminished buffering capacity during post-inflection destabilization.*

**Fig. S6**

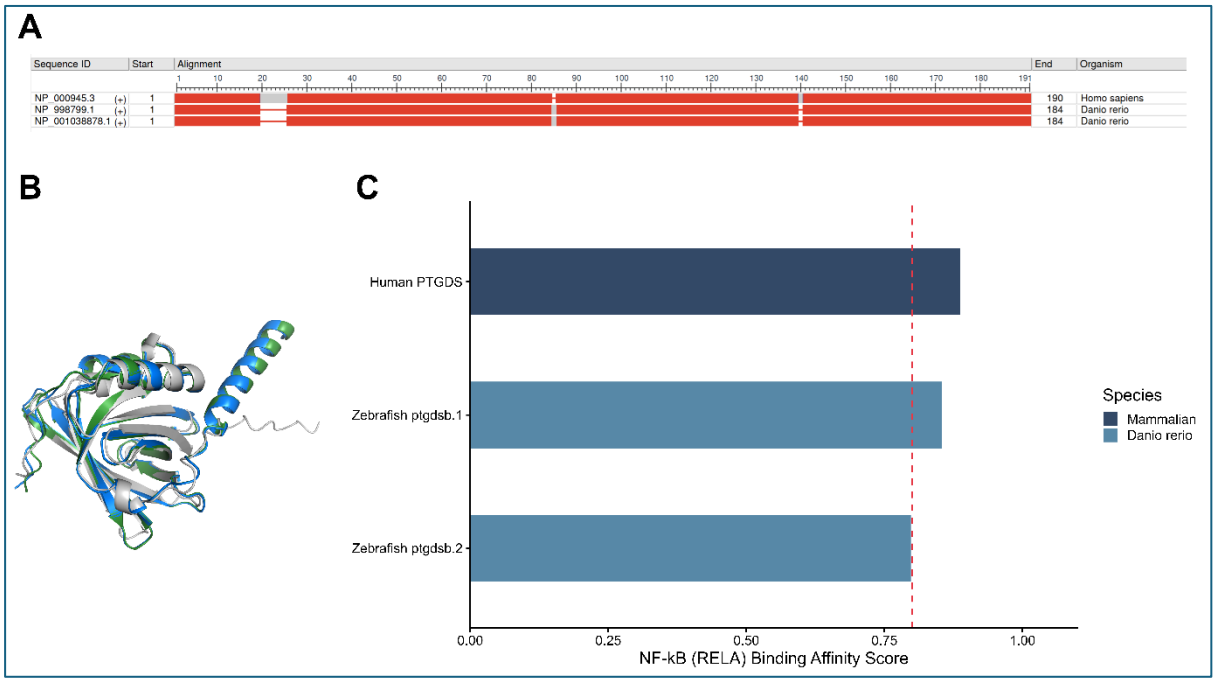


***Evolutionary conservation and structural homology of PTGDS.*** ***A.*** *Multiple sequence alignment of human PTGDS and zebrafish Ptgdsb.1/2. Red blocks indicate conserved residues, with the upper bar showing the conservation degree. Pairwise identity between human PTGDS and zebrafish Ptgdsb.1 is 85.6% (BLASTP).* ***B.*** *Structural superimposition of AlphaFold2-predicted PTGDS models. Zebrafish Ptgdsb.1 (marine) and Ptgdsb.2 (forest) show high similarity to human PTGDS (gray), with RMSD values of 1.10 Å and 1.23 Å, respectively.* ***C.*** *NF-κB (RELA) binding affinity scores for human and zebrafish ptgdsb promoters. The dashed red line denotes the significance threshold (0.8). *Data represent mean ± SEM of computational binding iterations. p < 0.05.*

**Fig. S7**

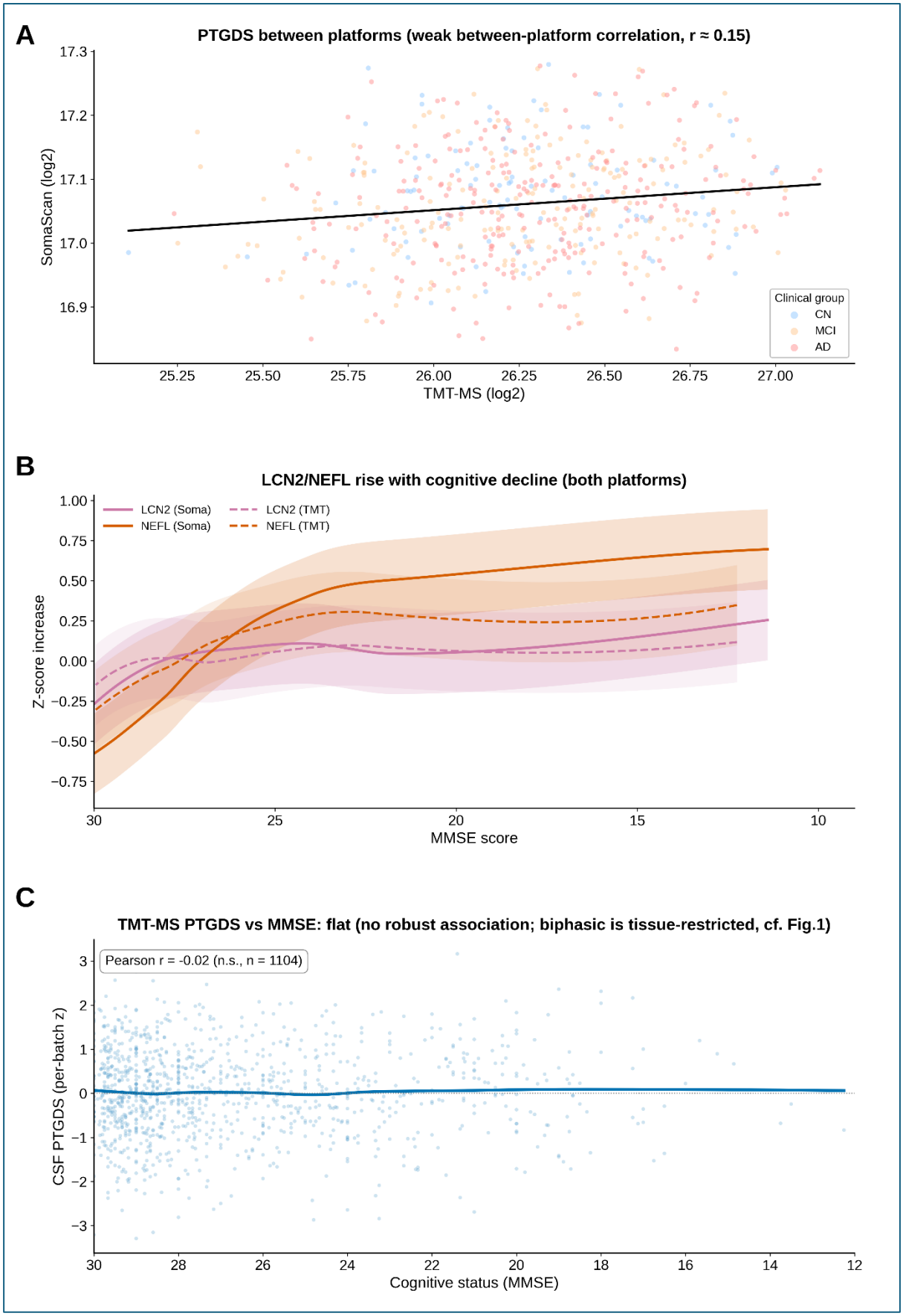
A
PTGDS between platforms (weak between-platform correlation, r ≈ 0.15)
SomaScan (log2)
TMT-MS (log2)
Clinical group
CN
MCI
AD
B
LCN2/NEFL rise with cognitive decline (both platforms)
LCN2 (Soma)
NEFL (Soma)
LCN2 (TMT)
NEFL (TMT)
Z-score increase
MMSE score
C
TMT-MS PTGDS vs MMSE: flat (no robust association; biphasic is tissue-restricted, cf. Fig.1)
Pearson r = -0.02 (n.s., n = 1104)
CSF PTGDS (per-batch z)
Cognitive status (MMSE)

***Cross-platform comparison of CSF biomarkers (ADNI; TMT-MS and SomaScan). A.*** *Platform-level comparison (PTGDS). At the individual-sample level, CSF PTGDS shows only weak correlation between TMT-MS and SomaScan (Pearson r ≈ 0.15, n = 580; below the threshold for cross-platform concordance); the panel reflects population-level distribution only, and upstream PTGDS is therefore considered tissue-restricted (cf. Fig. 1).* ***B.*** *CSF LCN2 and NEFL increase with progression on both platforms; NEFL is the strongest positive control (vs pathology axis r = +0.48 [TMT], clearing the |r| > 0.3 threshold; +0.24 [SomaScan], sub-threshold).* ***C.*** *Cognitive-decline inflection. CSF NEFL rises strongly with cognitive decline (the strongest CSF signal; r = −0.35), though a discrete breakpoint is not sharply localized; CSF PTGDS does not show a robust biphasic peak, consistent with the biphasic signal being restricted to brain tissue.*

**Fig. S8**

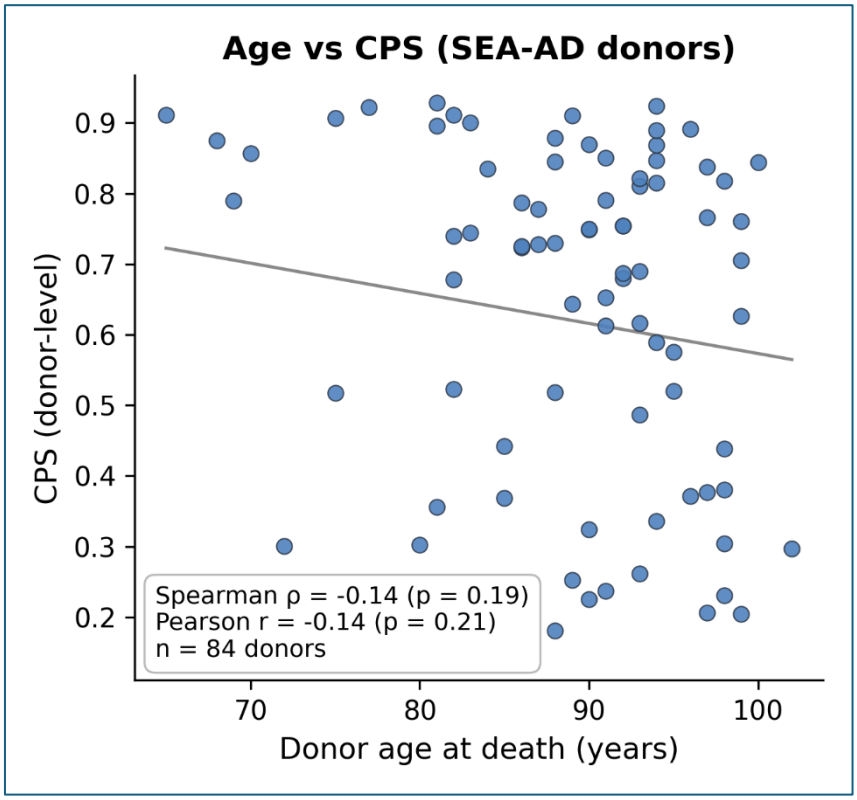


***Donor age at death is not correlated with pseudo-progression (CPS) in SEA-AD.*** *Donor-level scatter of chronological age at death versus CPS across all 84 SEA-AD donors (median age 90 years, range 65–102; ages uncensored). Spearman ρ = −0.14 (p = 0.19); Pearson r = −0.14 (p = 0.21). The weak, non-significant association confirms that CPS indexes neuropathological disease progression rather than chronological age; the astrocytic PTGDS inflection (CPS 0.47) therefore reflects disease-stage dynamics within a uniformly aged cohort rather than an age-driven change.*

## Table S1. Quality control metrics and bin-to-Braak stage mapping

### A. Bin-resolved cell type counts across pseudo-progression

| CPS Bin | Astrocyte | Exc. Neuron | SST+ Neuron | Microglia | Subtotal (4 types) | Total (all cells) | Approx. Braak Stage |
|---|---|---|---|---|---|---|---|
| 0.1 | 428 | 8,434 | 1,068 | 851 | 10,781 | 15,939 | ~I–II |
| 0.2 | 4,787 | 70,700 | 6,195 | 3,462 | 85,144 | 132,173 | ~I–II |
| 0.3 | 7,299 | 67,516 | 5,673 | 3,425 | 83,913 | 126,683 | ~I–II |
| 0.4 | 5,360 | 69,473 | 5,816 | 3,130 | 83,779 | 125,139 | ~III–IV |
| 0.5 | 4,691 | 48,108 | 2,981 | 3,203 | 58,983 | 89,488 | ~III–IV |
| 0.6 | 5,326 | 58,576 | 3,434 | 3,016 | 70,352 | 103,978 | ~III–IV |
| 0.7 | 11,656 | 113,320 | 7,922 | 6,823 | 139,721 | 211,778 | ~V–VI |
| 0.8 | 14,108 | 139,850 | 8,563 | 8,804 | 171,325 | 257,308 | ~V–VI |
| 0.9 | 13,764 | 95,712 | 5,557 | 6,191 | 121,224 | 178,422 | ~V–VI |

***Note:*** *Cell counts represent nuclei passing quality control from the SEA-AD middle temporal gyrus snRNA-seq atlas (84 donors). Exc. Neuron = all excitatory neuron subclasses (L2/3 IT, L5 ET, L6 CT, L6b, NP). SST+ Neuron = somatostatin-positive inhibitory interneurons. Subtotal includes the four analyzed cell types; Total includes all cell types in the atlas (oligodendrocytes, OPCs, endothelial, etc.). The tilde (~) prefix denotes approximate correspondence; Braak stage mapping is heuristic and does not imply direct pathological equivalence.*

### B. Quality control criteria

| Parameter | Criterion / Value |
|---|---|
| Minimum genes per nucleus | ≥ 500 |
| Maximum mitochondrial read fraction | < 20% |
| Doublet removal method | Scrublet-based (Wolock et al., 2019) |
| Atlas version | SEA-AD MTG snRNA-seq (2024-02-13) |
| Brain region | Middle temporal gyrus (MTG) |
| Total donors | 84 |
| Total nuclei (post-QC) | 1,240,908 |

### C. CPS-to-Braak stage mapping with aggregated cell counts

| Braak Stage (approx.) | CPS Bins | Total Cells | Astrocyte | Exc. Neuron | SST+ Neuron | Microglia |
|---|---|---|---|---|---|---|

| | | | | | | |
|---|---|---|---|---|---|---|
| ~I–II (Preclinical) | 0.1–0.3 | 274,795 | 12,514 | 146,650 | 12,936 | 7,738 |
| ~III–IV (Prodromal MCI) | 0.4–0.6 | 318,605 | 15,377 | 176,157 | 12,231 | 9,349 |
| ~V–VI (Dementia) | 0.7–0.9 | 647,508 | 39,528 | 348,882 | 22,042 | 21,818 |
| **Total** | — | 1,240,908 | 67,419 | 671,689 | 47,209 | 38,905 |

***Note:*** *CPS-to-Braak mapping is an approximate heuristic alignment for interpretive purposes: CPS 0.1–0.3 corresponds approximately to Braak stages I–II (preclinical to early symptomatic), CPS 0.4–0.6 to Braak III–IV (prodromal MCI spectrum), and CPS 0.7–0.9 to Braak V–VI (dementia). This mapping does not imply direct pathological equivalence, as CPS is derived from transcriptomic pseudo-progression rather than neuropathological staging. The tilde (~) prefix is used throughout to emphasize the approximate nature of this correspondence.*

**Table S2. Antibody & Primer Resources**

**Resources used for immunofluorescence staining and quantitative RT-PCR (qRT-PCR) in zebrafish and murine experiments.**

**A. qRT-PCR Primer Sequences — Zebrafish (Danio rerio)**

| Gene | Symbol | Dir. | Sequence (5'→3') | Tm (°C) | bp | Role / Panel |
|---|---|---|---|---|---|---|
| **ptgdsb.1** | ptgdsb.1 | F | AATGACAATGACATGCGCGT | 63 | 154 | Fig. 2F — astrocytic PTGDS (compensatory induction) |
| | | R | ACTGCCTGAACTTCTCCTTCA | | | |
| **ptgdsb.2** | ptgdsb.2 | F | GCCACATTTGACAAGTACGC | 63 | 127 | Fig. 2F — PTGDS paralogue |
| | | R | ACTGCCTGAACTTCTCCTTCA | | | |
| **ngfr** | ngfr | F | TGTGTGCAGTGTCCTCCAG | 64 | 125 | Fig. 2F/H — Neurogenic marker |
| | | R | ACCTGGCATTTGTCTGTGTG | | | |
| **bdnf** | bdnf | F | AGGAGTTGCTTGAGGTGGAA | 64 | 121 | Fig. 2F — Neurotrophic support |
| | | R | GAGGCATACAGGTCAACGTC | | | |
| **gfap** | gfap | F | CGGCTGGAGATTGAGAGAGA | 60 | 108 | Reactive gliosis marker |

| | | | | | | |
|---|---|---|---|---|---|---|
| | | R | GGTGTTGAGGTTATTTTCTGCCTC | | | |
| **tnf-α** | tnfa | F | AGGAACAAGTGCTTATGAGCCATGC | 60 | 157 | Fig. 2G — Pro-inflammatory |
| | | R | AAATGGAAGGCAGCGCCGAG | | | |
| **il-1β** | il1b | F | AGTAACCTGTACCTGGCCTGCAGC | 61 | 159 | Fig. 4C — Pro-inflammatory |
| | | R | GGTGTTTATGGAGCTGCCGGTCTC | | | |
| **il-6** | il6 | F | AAGGGGTCAGGATCAGCAC | 61 | 95 | Fig. 2G — Pro-inflammatory |
| | | R | GCTGTAGATTCGCGTTAGACATC | | | |
| **cox2 (ptgs2a)** | ptgs2a | F | AACTAGGATTCCAAGACGCAGCATC | 60 | 207 | Fig. 3 — Network pharmacology hub |
| | | R | AAATAAGAATGATGGCCGGAAGG | | | |
| **creb** | creb | F | GCACCACCATCCTGCAGTAT | 64 | 116 | Fig. 2F — Synaptic plasticity |
| | | R | AGTGCGGATCTGATAAGCCTG | | | |
| **dlg4 (psd-95)** | dlg4 | F | TGTCAGTCTGCAGGTGATGA | 64 | 151 | Fig. 2F — Synaptic integrity |
| | | R | GTGTGAGAGCTCTACCTGCC | | | |
| **nestin** | nes | F | AGCCAGCGTCAGGTACAG | 60 | 247 | Fig. 2C/D — Neural progenitor |
| | | R | TGTATGTTGCCACCTCCAGT | | | |
| **rplp0** | rplp0 | F | CTGAACATCTCGCCCTTCTC | 60 | 161 | Reference gene |
| | | R | TAGCCGATCTGCAGACACAC | | | |

***Note:*** *Zebrafish (Danio rerio) primers designed by Primer3; verified by NCBI Primer-BLAST. qRT-PCR: CFX96 Touch (Bio-Rad). Conditions: 95°C 3 min; 40 cycles of 95°C 10 s + Tm 30 s + 72°C 20 s. Relative expression normalized to rplp0 ($2^{-}\Delta\Delta Ct$). Tissue collected at 14 dpf and 21 dpf.*

## B. Antibodies for Whole-Mount Immunofluorescence (WIF) — Zebrafish

| Target | Description | Host | Supplier | Cat. No. | Dilution | Application / Panel |
|---|---|---|---|---|---|---|
| **Primary Antibodies** | | | | | | |
| **GFAP** | Anti-GFAP [ZRF-1] — Astrocyte Marker | Mouse | Abcam | ab154474 | **1:200** | Reactive gliosis; WIF (Fig. 2C) |
| **NGFR (p75NTR)** | Anti-p75NTR Neurotrophin Receptor Antibody | Rabbit | Merck | 07-476 | **1:100** | Neurogenic marker; WIF (Fig. 2D) |
| **BLBP (FABP7)** | Anti-BLBP antibody | Rabbit | Abcam | ab32423 | **1:200** | Astrocyte progenitor; WIF (Fig. 2C) |
| **Nestin** | Anti-Nestin antibody, clone 10C2 | Mouse | Merck | MAB5326 | **1:200** | Neural progenitor; WIF (Fig. 2D) |
| **Secondary Antibodies** | | | | | | |
| **Anti-Rabbit IgG (TRITC)** | Goat Anti-Rabbit IgG H&L (TRITC) | Goat | Abcam | ab6718 | **1:500** | 2° for Rabbit 1° (BLBP, NGFR) → Red channel |
| **Anti-Mouse IgG (AF488)** | Goat Anti-Mouse IgG H&L (Alexa Fluor® 488) | Goat | Abcam | ab150113 | **1:500** | 2° for Mouse 1° (GFAP, Nestin) → Green channel |

***Note:*** *WIF performed on 14 dpf larvae fixed in 4% PFA (overnight, 4°C). Blocking: 5% normal goat serum + 0.3% Triton X-100 in PBS (1 h, RT). Primary Ab: 48 h at 4°C; Secondary Ab: 2 h at RT, protected from light. Imaging: confocal microscope; fluorescence intensity quantified by ImageJ fixed ROI analysis. n = 10 larvae/group. IACUC: KW-241104-1; ZEFIT-IACUC-26010601-0001.*

**C. qRT-PCR Primer Sequences — Murine (Mus musculus, Aβ1–42 Mouse Model, Fig. 4)**

| Gene (Human) | Mouse Gene | Dir. | Sequence (5'→3') | Tm (°C) | Role / Panel |
|---|---|---|---|---|---|
| **LCN2** | Lcn2 | **F** | 5'-GGG AGA ACC AAG GAG CTG AC-3' | 57 | Inflammatory amplifier — Fig. 4C |
| | | **R** | 5'-CAG GGA GGC CCA GAG ATT TG-3' | | |
| **Keap1** | Keap1 | **F** | 5'-ATC TTC GAG GAG CTC ACC CT-3' | 57 | Oxidative stress / Nrf2 regulator — Fig. 4F |
| | | **R** | 5'-ATA CAG TTG TGC AGG ACG CA-3' | | |
| **NGFR** | Ngfr | **F** | 5'-TAT TGC TCC ATC CTG GCT GC-3' | 57 | Trophic / neurogenic marker — Fig. 4E |

| | | | | | |
|---|---|---|---|---|---|
| | | R | 5'-GAG TCT ATG TGC TCG GGC TG-3' | | |
| **BDNF** | Bdnf | F | 5'-TTT GGT TGC ATG AAG GCT GC-3' | 57 | Neurotrophic support — Fig. 4E |
| | | R | 5'-GCC GAA CTT TCT GGT CCT CA-3' | | |
| **APOE** | Apoe | F | 5'-CGT TGC TGG TCA CAT TCC TG-3' | 57 | Lipid transport — Fig. 4F |
| | | R | 5'-AAT CCC AAA AGC GAC CCA GT-3' | | |
| **ABCA1** | Abca1 | F | 5'-GCT GGT GTG GAC CCT TAC TC-3' | 57 | Lipid efflux transporter — Fig. 4F |
| | | R | 5'-GCA GCT TCA TAT GGC AGC AC-3' | | |
| **IL-6** | Il6 | F | 5'-GAG GAT ACC ACT CCC AAC AGA CC-3' | 57 | Pro-inflammatory cytokine — Fig. 4C |
| | | R | 5'-AAG TGC ATC ATC GTT GTT CAT ACA-3' | | |
| **IL-1β** | Il1b | F | 5'-ACC TGC TGG TGT GTG ACG TT-3' | 57 | Pro-inflammatory cytokine — Fig. 4C |
| | | R | 5'-TCG TTG CTT GGT TCT CCT TG-3' | | |
| **TNF-α** | Tnf | F | 5'-AGC ACA GAA AGC ATG ATC CG-3' | 57 | Pro-inflammatory cytokine — Fig. 4C |
| | | R | 5'-CTG ATG AGA GGG AGG CCA TT-3' | | |
| **β-actin** | Actb | F | 5'-ATC ACT ATT GGC AAC GAG CG-3' | 57 | Reference gene |
| | | R | 5'-TCA GCA ATG CCT GGG TAC AT-3' | | |

***Note:*** *Mouse primers for Mus musculus (ICR, male, 5 weeks). RNA extracted from hippocampal tissue using TRIzol (Invitrogen). cDNA synthesis: All-in-One First-Strand cDNA Synthesis SuperMix (TransGen Biotech). RT-qPCR: QuantStudio 3 (Applied Biosystems) with PowerSYBR® Green PCR Master Mix (Thermo Fisher). Cycling: 95°C 15 s → 57°C 20 s → 72°C 40 s, 40 cycles. Relative expression normalized to β-actin (Actb) by $2^{-}\Delta\Delta Ct$ method.*

**Table S3. Summary of Behavioral Test Results in Aβ-injected Mouse Model**

| Experimental Group | n | Y-maze | p vs | p vs Aβ | PAT Retention | p vs | p vs Aβ |
|---|---|---|---|---|---|---|---|

| | | Alternation (%) | Sham | | Latency (s) | Sham | |
|---|---|---|---|---|---|---|---|
| Sham (Control) | 10 | 67.4 ± 3.16 | — | — | 189.0 ± 30.62 | — | — |
| Aβ (20 μM) | 9† | 53.3 ± 4.37 | * | — | 67.9 ± 19.36 | *** | — |
| Aβ + BXP-101 (50 mg/kg) | 10 | 57.7 ± 2.19 | ns | ns | 168.7 ± 32.28 | ns | ** |
| Aβ + BXP-101 (100 mg/kg) | 10 | 61.3 ± 2.52 | ns | ns | 155.2 ± 37.26 | ns | * |
| Aβ + BXP-101 (200 mg/kg) | 10 | 64.6 ± 3.44 | ns | ns | 181.9 ± 36.54 | ns | *** |
| Aβ + BXP-101 (400 mg/kg) | 10 | 66.1 ± 2.08 | ns | * | 221.0 ± 22.05 | ns | *** |
| Aβ + Donepezil (5 mg/kg) | 10 | 66.7 ± 2.79 | ns | * | 180.9 ± 29.92 | ns | *** |

***Note:*** *Values are presented as Mean ± SEM. Y-maze Alternation (%): Measures spatial working memory based on the percentage of spontaneous alternations in a Y-shaped maze (One-Way ANOVA, Newman-Keuls post hoc). PAT (Passive Avoidance Test) Retention Latency: Measures long-term associative memory based on the time (seconds) to enter a dark compartment where an electric shock was previously delivered (Two-Way ANOVA, Bonferroni post hoc). †Aβ group: n = 9 (1 animal excluded as outlier); all other groups n = 10. Aβ: Amyloid-beta 1–42 (20 μM) intracerebroventricularly (i.c.v.) injected to induce AD-like cognitive impairment. BXP-101: A standardized multi-herbal extract administered orally for 4 weeks. Donepezil (DNZ): Used as a positive reference control. *p < 0.05, **p < 0.01, ***p < 0.001; ns, not significant.*

**Table S4. Bin-resolved cell-type-specific expression trajectories across the CPS continuum**

**1. Astrocyte Trajectories**

| CPS Bin | n cells | NDUFS1 | PTGDS | LCN2 | APOE | TREM2 | C3 | NFKBIA | CLU | GFAP |
|---|---|---|---|---|---|---|---|---|---|---|
| 0.1 | 428 | 0.5792 | 1.6531 | 0.0000 | 0.8090 | 0.0002 | 0.1987 | 0.1790 | 2.1115 | 1.8767 |
| 0.2 | 4,787 | 0.5742 | 1.7275 | 0.0000 | 0.8364 | 0.0003 | 0.1594 | 0.1606 | 2.1245 | 1.6573 |
| 0.3 | 7,299 | 0.5610 | 1.8725 | 0.0000 | 0.9853 | 0.0006 | 0.1346 | 0.1541 | 2.2025 | 1.6725 |
| 0.4 | 5,360 | 0.5486 | 1.8805 | 0.0001 | 0.9480 | 0.0006 | 0.1203 | 0.1539 | 2.1821 | 1.8061 |
| 0.5 | 4,691 | 0.5566 | 1.9290 | 0.0001 | 0.9986 | 0.0005 | 0.1190 | 0.1697 | 2.1813 | 1.8907 |
| 0.6 | 5,326 | 0.5739 | 1.8941 | 0.0001 | 0.9354 | 0.0006 | 0.1067 | 0.1694 | 2.1526 | 1.7501 |
| 0.7 | 11,656 | 0.5864 | 1.8430 | 0.0000 | 0.9255 | 0.0007 | 0.0961 | 0.1698 | 2.1600 | 1.4806 |
| 0.8 | 14,108 | 0.5791 | 1.6735 | 0.0001 | 0.8009 | 0.0009 | 0.1179 | 0.1823 | 2.1836 | 1.6310 |
| 0.9 | 13,764 | 0.5769 | 1.6310 | 0.0001 | 0.7428 | 0.0009 | 0.1171 | 0.1805 | 2.2026 | 1.7018 |

**2. Neuronal Trajectories (Excitatory & SST)**

| CPS Bin | Cell Type | n cells | NDUFS1 | PTGDS | NGFR | APOE | BDNF | SLC22A17 |
|---|---|---|---|---|---|---|---|---|
| 0.1 | Exc_Neuron | 8,434 | 0.7817 | 0.0810 | 0.0026 | 0.0287 | 0.2929 | 0.4751 |
| 0.5 | Exc_Neuron | 48,108 | 0.6952 | 0.0848 | 0.0005 | 0.0218 | 0.1053 | 0.4347 |
| 0.9 | Exc_Neuron | 95,712 | 0.7061 | 0.0910 | 0.0007 | 0.0269 | 0.0754 | 0.4197 |
| 0.1 | SST_Neuron | 1,068 | 0.6704 | 0.0818 | 0.0004 | 0.0381 | 0.0100 | 0.4084 |
| 0.5 | SST_Neuron | 2,981 | 0.5580 | 0.1067 | 0.0003 | 0.0328 | 0.0051 | 0.4349 |
| 0.9 | SST_Neuron | 5,557 | 0.5356 | 0.1115 | 0.0005 | 0.0344 | 0.0031 | 0.3955 |

## 3. Microglia Trajectories

| CPS Bin | n cells | APOE | TREM2 | C3 | NFKBIA | GPX4 | FTH1 |
|---|---|---|---|---|---|---|---|
| 0.1 | 851 | 1.1820 | 0.2363 | 1.1598 | 0.1571 | 0.1750 | 1.8107 |
| 0.5 | 3,203 | 1.1277 | 0.2599 | 1.6931 | 0.2454 | 0.2025 | 1.1718 |
| 0.9 | 6,191 | 1.2186 | 0.2309 | 1.5007 | 0.3141 | 0.2150 | 0.8985 |

***Note:*** *Expression values represent 3-bin moving average (MA) of log-normalized expression from the SEA-AD atlas. Cell types: Astrocyte, Exc_Neuron (excitatory neurons), SST_Neuron (somatostatin-positive inhibitory interneurons), Microglia. LCN2 detection rate in astrocytes was 0.007% (5/67,419); values near zero should be interpreted cautiously. Raw (unsmoothed) per-bin peak for PTGDS = 2.02 at Bin 0.6; the 3-bin moving-average peak falls at Bin 0.5 (1.93). The quadratic vertex estimated at the donor level (CPS 0.47, bootstrap 95% CI 0.32–0.53) therefore lies below the raw bin maximum, as expected when a symmetric parabola is fitted to an asymmetric trajectory with unequal donor coverage across bins (Table S5). Donor counts per bin are highly uneven: Bin 0.1 comprises a single donor.*

## Table S5. Donor counts per CPS bin and robustness of the PTGDS inflection

**A. Donor and astrocyte counts per CPS bin**

| CPS bin | Donors | Astrocytes | PTGDS (donor mean) | Note |
|---|---|---|---|---|
| 0.1 | 1 | 428 | 1.4281 | Single donor (CPS 0.150); lowest observed CPS |
| 0.2 | 9 | 4,787 | 1.8608 | |
| 0.3 | 8 | 7,299 | 1.8524 | |
| 0.4 | 7 | 5,360 | 1.8972 | |
| 0.5 | 5 | 4,691 | 1.9218 | Moving-average peak |
| 0.6 | 6 | 5,326 | 1.9636 | Unsmoothed raw peak (cell-weighted 2.0219) |
| 0.7 | 14 | 11,656 | 1.7785 | |
| 0.8 | 17 | 14,108 | 1.8086 | |
| 0.9 | 17 | 13,764 | 1.4784 | |

| | | | | |
|---|---|---|---|---|
| **Total** | **84** | **67,419** | — | — |

***Note:*** *Donor counts are markedly uneven across the CPS range. Bin 0.1 contains a single donor (428 astrocytes) and the observed CPS range does not extend below 0.150, so the earliest portion of the trajectory is sparsely sampled. PTGDS values shown are donor-level means within each bin; the cell-weighted bin means reported in Table S4 differ slightly because donors contribute unequal numbers of nuclei. All inferential statistics in Table 2 are computed at the donor level (n = 84).*

**B. Robustness of the quadratic inflection**

**Leave-one-donor-out.** The quadratic was refitted 84 times, each time omitting one donor. Curvature remained significant in every refit ($\beta_2$ −2.506 to −2.015; p 0.0022–0.0145; vertex 0.456–0.489). Omission of the single donor occupying bin 0.1 (CPS 0.150) gave $\beta_2 = -2.069$, p = 0.0145. The curvature is therefore not attributable to any individual donor.

**Low-CPS truncation.** Refitting after removing the lowest-CPS donors preserved the curvature: CPS ≥ 0.16 (n = 83) $\beta_2 = -2.069$, p = 0.0145; CPS ≥ 0.20 (n = 80) $\beta_2 = -2.387$, p = 0.0097; CPS ≥ 0.25 (n = 74) $\beta_2 = -2.495$, p = 0.0295. The inflection is not an artefact of the sparsely sampled low-CPS edge.

**Vertex bootstrap.** Resampling donors 10,000 times gave a vertex 95% confidence interval of 0.32–0.53 (point estimate 0.472); 98.9% of resampled vertices fell inside the observed CPS range and 99.8% yielded $\beta_2 < 0$. The inflection position is bounded away from both ends of the range but spans approximately two CPS bins, and CPS 0.47 should therefore be read as the centroid of an interval rather than a precise threshold.

**Limb asymmetry.** Fitting separate linear slopes either side of the vertex gave a robust descending limb (CPS > 0.47: slope −1.212, p = 0.0027, n = 59) and an ascending limb that did not reach significance in any window tested (CPS ≤ 0.47: slope +0.496, p = 0.445, n = 25; excluding the single lowest-CPS donor: slope +0.160, p = 0.811, n = 24; CPS 0.20–0.47: slope +0.441, p = 0.543, n = 21). The curvature and the descending limb are statistically supported; a preceding compensatory rise is directionally consistent but is not established at donor level.

**Model comparison.** By AIC the quadratic (−182.2) was preferred over a linear model (−176.2) and over a plateau-then-decline hinge model (−180.8; fitted breakpoint 0.66), although the margin over the hinge model is small (ΔAIC 1.4) and does not exclude it.

**Reproducibility.** All values in this table were generated from the donor-level dataset deposited at https://github.com/YoungOukKim/MCI-to-AD using the analysis script P1_vertex_CI_and_sensitivity.R (set.seed(42)).

**Table S6. Spearman correlations of apoptotic, identity, and reactive markers with CPS in astrocytes**

| Marker | Category | Spearman Rho | p-value | n |
|---|---|---|---|---|
| CASP3 | Apoptotic | −0.229 | 0.036 | 84 |
| BAX | Apoptotic | −0.130 | 0.236 | 84 |
| BCL2 | Apoptotic | +0.299 | 0.006 | 84 |
| SLC1A2 | Identity | −0.020 | 0.857 | 84 |
| AQP4 | Identity | −0.213 | 0.052 | 84 |
| GFAP | Reactive | +0.105 | 0.343 | 84 |

***Note:*** *Spearman correlations in this table are computed at the donor level (n = 84 donors); a prior cell-*

*level computation (n = 67,419 nuclei) inflated significance and is superseded. At the superseded cell level, apoptotic markers (CASP3, BAX) showed negligible correlations with CPS (|ρ| < 0.03), indicating that PTGDS decline reflects functional state reprogramming rather than astrocyte population loss. Identity markers (SLC1A2, AQP4) showed small negative correlations (|ρ| < 0.08), consistent with preserved but modestly declining astrocyte identity. Reactive markers (GFAP, NFKBIA) showed modest positive correlations, consistent with phenotypic transition toward reactive gliosis. At the donor level, anti-apoptotic BCL2 increases (ρ = +0.30, p = 0.006; the only marker surviving multiple-testing correction), pro-apoptotic CASP3/BAX do not increase, AQP4 shows a marginal decline (ρ = −0.21, p = 0.05), and GFAP is not significant (ρ = +0.10, n.s.); NFKBIA is characterized at the module/trajectory level (Table S9).*

**Table S7. Lagged cross-correlation analysis across the full CPS trajectory (Bins 0.1–0.9)**

| Interaction Pair | Lag (Bins) | r-value | p-value | n_eff |
|---|---|---|---|---|
| Purinergic → PTGDS | −3 | −0.7250 | 0.2755 | 4 |
| NF-κB → PTGDS | −1 | −0.7060 | 0.1167 | 6 |
| PTGDS → PPARG | −2 | 0.5570 | 0.3298 | 5 |
| C3 → NGFR | 0 | −0.9340 | 0.0021 | 7 |
| NDUFS1 → PTGDS | −3 | 0.7440 | 0.2563 | 4 |

***Note:*** *Lagged cross-correlations on 3-bin moving-average trajectories across the full CPS range (Bins 0.1–0.9, n = 9 bins, lag.max = 3). Negative lag denotes a descriptive temporal offset only; with limited effective sample size after lagging (n_eff = 3–7) and moving-average-induced autocorrelation, lead–lag ordering cannot establish causal direction and p-values are exploratory. Apparent associations (e.g., C3–NGFR r = −0.934) are reported as hypotheses consistent with complement-mediated neurotoxicity and metabolic-crisis coupling. Astrocytic LCN2 pairs were excluded because LCN2 was detected in only 0.007% of astrocytes (5/67,419); the LCN2 arm is instead supported by CSF/qPCR. For inflection-window analysis (Bins 0.4–0.8), see Table 3 in main text.*

**Table S8. Neuronal subtype-specific expression and vulnerability across CPS bins**

| CPS Bin | Subtype | n cells | NDUFS1 (mean) | NDUFS1 (var) | NGFR (mean) | BCL2 (mean) | BAX (mean) | CASP3 (mean) | BAX/BCL2 | SST % | Exc % |
|---|---|---|---|---|---|---|---|---|---|---|---|
| 0.1 | Exc | 8,434 | 0.8316 | 0.1579 | 0.0048 | 0.7583 | 0.0372 | 0.0898 | 0.0491 | 11.24 | 88.76 |
| 0.2 | Exc | 70,700 | 0.7317 | 0.1283 | 0.0005 | 0.8158 | 0.0439 | 0.1058 | 0.0538 | 8.06 | 91.94 |
| 0.3 | Exc | 67,516 | 0.7438 | 0.1294 | 0.0006 | 0.7523 | 0.0369 | 0.1077 | 0.0490 | 7.75 | 92.25 |
| 0.4 | Exc | 69,473 | 0.7101 | 0.1280 | 0.0006 | 0.7765 | 0.0490 | 0.1029 | 0.0631 | 7.72 | 92.28 |
| 0.5 | Exc | 48,108 | 0.6860 | 0.1182 | 0.0006 | 0.7375 | 0.0356 | 0.1021 | 0.0483 | 5.83 | 94.17 |
| 0.6 | Exc | 58,576 | 0.6896 | 0.1342 | 0.0005 | 0.7533 | 0.0334 | 0.0981 | 0.0443 | 5.54 | 94.46 |
| 0.7 | Exc | 113,320 | 0.7269 | 0.1333 | 0.0008 | 0.7632 | 0.0385 | 0.1051 | 0.0505 | 6.53 | 93.47 |

| | | | | | | | | | | | |
|---|---|---|---|---|---|---|---|---|---|---|---|
| 0.8 | Exc | 139,850 | 0.7151 | 0.1464 | 0.0007 | 0.7621 | 0.0333 | 0.1017 | 0.0438 | 5.77 | 94.23 |
| 0.9 | Exc | 95,712 | 0.6971 | 0.1626 | 0.0007 | 0.6547 | 0.0304 | 0.1036 | 0.0465 | 5.49 | 94.51 |
| 0.1 | SST | 1,068 | 0.7418 | 0.1899 | 0.0003 | 0.6426 | 0.0231 | 0.1267 | 0.0360 | 11.24 | 88.76 |
| 0.2 | SST | 6,195 | 0.5990 | 0.2533 | 0.0006 | 0.6205 | 0.0313 | 0.1148 | 0.0504 | 8.06 | 91.94 |
| 0.3 | SST | 5,673 | 0.6105 | 0.2525 | 0.0005 | 0.5520 | 0.0265 | 0.1236 | 0.0480 | 7.75 | 92.25 |
| 0.4 | SST | 5,816 | 0.5823 | 0.2346 | 0.0001 | 0.5992 | 0.0344 | 0.1159 | 0.0575 | 7.72 | 92.28 |
| 0.5 | SST | 2,981 | 0.5489 | 0.2610 | 0.0005 | 0.4967 | 0.0269 | 0.1029 | 0.0541 | 5.83 | 94.17 |
| 0.6 | SST | 3,434 | 0.5428 | 0.2555 | 0.0004 | 0.5790 | 0.0242 | 0.1200 | 0.0418 | 5.54 | 94.46 |
| 0.7 | SST | 7,922 | 0.5687 | 0.2480 | 0.0005 | 0.5621 | 0.0243 | 0.1145 | 0.0432 | 6.53 | 93.47 |
| 0.8 | SST | 8,563 | 0.5571 | 0.2627 | 0.0005 | 0.5527 | 0.0236 | 0.1132 | 0.0428 | 5.77 | 94.23 |
| 0.9 | SST | 5,557 | 0.5142 | 0.2567 | 0.0005 | 0.5942 | 0.0215 | 0.1172 | 0.0362 | 5.49 | 94.51 |

***Note:*** *Neuronal subtype-specific expression across CPS bins from the SEA-AD atlas. Values in this table are unsmoothed per-bin means; Table S4 and main-text Table 1 report 3-bin moving averages of the same data, so corresponding entries differ (for example excitatory NGFR at Bin 0.1 is 0.0048 here and 0.0026 after smoothing). Excitatory = all excitatory neuron subclasses (L2/3 IT, L5 ET, L6 CT, L6b, NP). SST = somatostatin-positive inhibitory interneurons. SST interneurons declined from 11.24% (Bin 0.1, n = 1,068) to 5.49% (Bin 0.9, n = 5,557), representing a 51.2% proportional reduction (as a fraction of excitatory + SST neurons; donor-level Spearman ρ = −0.32, p = 0.003). SST neurons exhibited higher NDUFS1 variance (0.19–0.26) compared to excitatory neurons (0.12–0.16), indicating increased metabolic heterogeneity. BAX/BCL2 ratio = BAX mean / (BCL2 mean + 1e-10) per bin, indexing apoptotic vulnerability.*

**Table S9. ADNI participant demographics**

| Characteristic | CN (n=172) | EMCI (n=183) | LMCI (n=234) | AD (n=146) | p-value |
|---|---|---|---|---|---|
| Age (years) | 74.5 ± 5.9 | 71.1 ± 7.3 | 73.2 ± 7.6 | 75.2 ± 8.5 | 0.002 |
| Female (%) | 46.5 | 42.6 | 42.3 | 41.8 | 0.42 |
| Education (years) | 16.3 ± 2.7 | 15.8 ± 2.7 | 16.0 ± 3.0 | 15.4 ± 2.9 | 0.03 |
| APOE ε4 carriers (%) | 25.0 | 45.4 | 58.1 | 69.2 | < 0.001 |
| MMSE | 29.0 ± 1.1 | 28.2 ± 1.6 | 26.8 ± 1.7 | 23.6 ± 2.0 | < 0.001 |

***Note:*** *Data presented as mean ± SD or percentage. p-values from ANOVA (continuous) or Chi-square test (categorical). CN = cognitively normal; EMCI = early MCI; LMCI = late MCI; AD = Alzheimer's disease. MMSE, Mini-Mental State Examination. APOE ε4 carrier status defined as at least one ε4 allele. CSF Aβ42 and p-Tau181 values used as covariates in ROC/Cox analyses were measured by Roche Elecsys immunoassay (UPENNBIOMK dataset).*

**Table S10. Independent brain bulk proteomic validation of PTGDS and the M25 metabolism module (Johnson et al., 2022; ROSMAP and Banner cohorts)**

**A. Individual-protein differential abundance (ROSMAP DLPFC, n = 84 control + 148 AsymAD + 108 AD; Banner DLPFC, n = 26 control + 58 AsymAD + 92 AD; combined n = 488; 8,619 proteins by TMT-MS)**

| Protein | $\log_2$(AD) − $\log_2$(Ctrl) | $\log_2$(AsymAD) − $\log_2$(Ctrl) | $\log_2$(AD) − $\log_2$(AsymAD) | ANOVA F | ANOVA P | Holm-adj P (AD vs Ctrl) | WGCNA module (kME) |
|---|---|---|---|---|---|---|---|
| **PTGDS** | +0.090 | +0.040 | +0.051 | 5.752 | $3.40 \times 10^{-3}$ | $2.64 \times 10^{-3}$ | M25 Sugar Metabolism (0.42) |
| **LCN2** | +0.093 | +0.020 | +0.073 | 1.479 | 0.230 | 0.290 | M41 Ambiguous (0.72) |

***Note:*** *PTGDS shows significant elevation in AD (Holm-corrected $p = 2.6 \times 10^{-3}$ across all 8,619 proteins). The pairwise Tukey contrast AsymAD vs Control did not reach significance (Holm-adj p = 0.17), whereas AD vs AsymAD was significant (Holm-adj p = 0.046), indicating progressive accumulation in symptomatic stages. The stage-wise Holm-adjusted values quoted here and in the main text (AsymAD vs Control p = 0.17; AD vs AsymAD p = 0.046) derive from the same Tukey/Holm output of the source dataset as the AD-vs-Control value tabulated above. LCN2 shows directionally concordant elevation with comparable effect size but markedly larger between-case variance (lower F statistic), consistent with the inducible NF-κB-regulated kinetics expected for an inflammatory amplifier and the secreted-protein detection limits inherent to bulk-tissue MS. All values extracted from Johnson et al. (2022), Supplementary Table 2 (sheet '2.Master.PD.cleanDat.Stat.kME').*

**B. M25 Sugar Metabolism module synthetic eigenprotein across cohorts and brain regions**

| Cohort / Brain region | Region annotation | ANOVA F | ANOVA P | Tukey P (AD vs Ctrl) | Avg diff $\log_2$(AD) − $\log_2$(Ctrl) |
|---|---|---|---|---|---|
| **Mt. Sinai BB BA-36** | Parahippocampal gyrus (temporal lobe) | 1.957 | 0.145 | 0.192 | +0.026 |
| **ROSMAP BA-6** | Frontal cortex | 2.667 | 0.074 | 0.067 | +0.011 |
| **ROSMAP BA-37** | Inferior temporal cortex | 5.612 | $4.80 \times 10^{-3}$ | $3.18 \times 10^{-3}$ | +0.017 |
| **Emory BA-9** | DLPFC (AD/PD design) | 1.854 | 0.171 | 0.272 | +0.095 |
| **Emory BA-24** | Anterior cingulate gyrus | 5.759 | $6.65 \times 10^{-3}$ | $7.79 \times 10^{-3}$ | +0.178 |

***Note:*** *Module-level upregulation in AD vs Control is significant (Tukey $p < 0.01$) in two of five tested regions: ROSMAP inferior temporal cortex (BA-37) and Emory anterior cingulate (BA-24). The strongest temporal-lobe signal occurs in BA-37, the region anatomically corresponding to the SEA-AD middle temporal gyrus atlas used for trajectory inference (Fig. 1). Values extracted from Johnson et al. (2022), Supplementary Table 17 (sheet '17.ANOVA.SynthEigenprotein').*

**C. Top-ranking M25 Sugar Metabolism module members by intramodular connectivity (kME); 20 of 104 members shown**

| Symbol | kME | $\log_2$(AD) − $\log_2$(Ctrl) | Holm-adj P (AD vs Ctrl) | Functional annotation |
|---|---|---|---|---|
| **DYNC1H1** | 0.724 | +0.0007 | 0.922 | Cytoplasmic dynein 1 heavy chain |
| **RUFY3** | 0.687 | +0.0120 | 0.299 | RUN/FYVE domain protein |
| **AHCY** | 0.683 | +0.0206 | 0.041 | Adenosylhomocysteinase (SAM cycle) |
| **GRHPR** | 0.682 | +0.0708 | $2.26 \times 10^{-12}$ | Glyoxylate/hydroxypyruvate reductase |
| **ACTR1A** | 0.681 | +0.0086 | 0.519 | Alpha-centractin |
| **DCTN1** | 0.671 | +0.0040 | 0.481 | Dynactin subunit 1 |
| **PGD** | 0.669 | +0.0537 | $4.32 \times 10^{-9}$ | 6-phosphogluconate dehydrogenase (pentose phosphate) |
| **TRIM2** | 0.662 | +0.0223 | 0.020 | Tripartite motif protein |
| **NUDT5** | 0.661 | +0.0482 | $1.45 \times 10^{-4}$ | ADP-sugar pyrophosphatase |
| **GGPS1** | 0.658 | +0.0250 | 0.058 | Geranylgeranyl pyrophosphate synthase (isoprenoid) |
| **ACSS2** | 0.655 | +0.0419 | $2.26 \times 10^{-3}$ | Acetyl-CoA synthetase, cytoplasmic |
| **GARS** | 0.644 | +0.0160 | 0.162 | Glycyl-tRNA synthetase |
| **UBA6** | 0.642 | +0.0192 | 0.043 | Ubiquitin-activating enzyme 6 |
| **GDI2** | 0.636 | +0.0145 | 0.336 | Rab GDP dissociation inhibitor beta |
| **TXNL1** | 0.635 | +0.0257 | 0.021 | Thioredoxin-like protein 1 |
| **DYNC1LI2** | 0.627 | +0.0251 | $4.44 \times 10^{-3}$ | Cytoplasmic dynein light intermediate chain 2 |
| **GLRX3** | 0.615 | +0.0319 | $4.48 \times 10^{-3}$ | Glutaredoxin-3 |
| **TARS** | 0.615 | +0.0277 | $2.37 \times 10^{-3}$ | Threonyl-tRNA synthetase |
| **MAP2K2** | 0.608 | +0.0258 | $5.47 \times 10^{-3}$ | MAP kinase kinase 2 (MEK2) |
| **FASN** | 0.578 | +0.0523 | $1.37 \times 10^{-6}$ | Fatty acid synthase (lipid biosynthesis) |

***Note:*** *PTGDS is rank 74 of 104 module members (kME = 0.4244). Module hubs include FASN (fatty acid synthesis), GGPS1 (isoprenoid biosynthesis), ACSS2 (acetyl-CoA metabolism), AHCY (SAM-cycle methylation supplying lipid biosynthesis), and PGD (pentose phosphate flux producing NADPH for lipogenesis), broadly metabolic in character. We note, however, that PTGDS is a peripheral member of this module (rank 74 of 104; kME = 0.4244) and that the highest-connectivity hubs are cytoskeletal and transport proteins (DYNC1H1, RUFY3, ACTR1A, DCTN1) rather than lipid-metabolic enzymes; the robust and reproducible observation in this dataset is the elevation of PTGDS itself rather than a coordinated module-level change, consistent with the main text. Values extracted from Johnson et al. (2022), Supplementary Table 2.*